To be submitted to
Nuclear Instr. & Meth.

ISTITUTO NAZIONALE DI FISICA NUCLEARE
Laboratori Nazionali di Frascati

LNF-84/20(P)
20 Aprile 1984

Yu.K. Akimov, F. Balestra, Yu.A. Batusov, G. Bendiscioli, M.P. Bussa, L. Busso, A. Cavestro, L. Ferrero, I.V. Falomkin, V. Filippini, G. Fumagalli, G. Gervino, A. Grasso, C. Guaraldo, E. Lodi Rizzini, A. Maggiora, C. Marciano, D. Panzieri, G. Piragino, G.B. Pontecorvo, A. Rotondi, F. Tosello, M. Vascon, A. Venaglioni, G. Zanella and A. Zenoni:
EXPERIMENTAL APPARATUS FOR STUDYING INTERACTION OF ANTIPROTONS WITH LIGHT NUCLEI.

Servizio Documentazione
dei Laboratori Nazionali di Frascati
Cas. Postale 13 - Frascati (Roma)

INFN - Laboratori Nazionali di Frascati
Servizio Documentazione

LNF-84/20(P)
20 Aprile 1984

EXPERIMENTAL APPARATUS FOR STUDYING INTERACTION OF ANTIPROTONS WITH LIGHT NUCLEI

F. Balestra, M.P. Bussa, L. Busso, L. Ferrero, G. Gervino, A. Grasso, D. Panzieri, G. Piragino, F. Tosello
Istituto di Fisica dell'Università di Torino and INFN, Sezione di Torino, Italy

G. Bendiscioli, V. Filippini, G. Fumagalli, E. Lodi Rizzini, C. Marciano, A. Rotondi, A. Venaglioni, A. Zenoni
Dipartimento di Fisica Nucleare e Teorica dell'Università di Pavia and INFN, Sezione di Pavia, Italy

C. Guaraldo, A. Maggiora
Laboratori Nazionali di Frascati dell'INFN, Frascati, Italy

A. Cavestro, M. Vascon, G. Zanella
Dipartimento di Fisica dell'Università di Padova and INFN, Sezione di Padova, Italy

Yu.K. Akimov, Yu. A. Batusov, I.V. Falomkin and G.B. Pontecorvo
Joint Institute for Nuclear Research, Dubna, USSR.

A description is given of the detector system (self-shunted streamer chamber in magnetic field) used in the PS 179 experiment at LEAR for studying antiproton interaction with light nuclei.

1. - INTRODUCTION

In this paper the experimental apparatus that was prepared for use in the study of the interactions of antiprotons with light nuclei at the LEAR facility[1] of CERN is described.

The physical aims of the PS 179 experiment have been described previously in detail[2] and, briefly, are based on the following: the experimental study of the interaction of antiprotons with nuclei at low energies will provide further information on the fundamental nucleon-antinucleon forces, the interaction of antiprotons with bound nucleons, the distribution of nuclear matter, and the properties of highly excited nuclear matter. One of the immediate objects of the experiment is the measurement of the effective yields of ^{3}He, ^{3}H and ^{2}H in $\bar{p}\,^4$He annihilation and, thus, the imposition of restrictions on the possible amount of antimatter in the early Universe[3], as well as on certain parameters of super symmetric models of grand unification[4].

In order to take the most of the information available on all the secondary particles produced in each individual event detected of antiproton-nucleus interactions we have chosen to profit from the advantageous properties of a self-shunted streamer chamber placed in a magnetic field, the chamber serving simultaneously as a low density gas target and a triggerable 4π-acceptance track detector in which higly luminous localized particle tracks are obtained[5].

2. - LAYOUT OF THE EXPERIMENTAL APPARATUS

The experimental apparatus mounted in the LEAR experimental hall is depicted in Fig. 1. It incorporates the streamer chamber (SC) itself which operates at a 1 atm pressure of the filling gas, the analyzing electromagnet (EM) and the triggering system, consisting of scintillation counters (C_{1-5}). Two proportional wire chambers ($WC_{1,2}$) have been used only for monitoring the beam structure and position. The intensity of the $\bar{p}$ beam passing through the chamber was 10^4÷5 x 10^4 s^{-1} at 610 MeV/c. The streamer chamber in the magnet (see Fig. 2), together with the high voltage pulse generator (HVPG), are situated inside a Faraday electrostatic screening cage (ES) made of copper mesh; this is a necessary step taken to not disturb the electronic equipments utilized by other numerous experiments present in the same experimental hall from electromagnetic noise when the high voltage pulse is applied to the streamer chamber. Pictures of $\bar{p}$ annihilation events occuring in the streamer chamber are taken by two photocameras (C) to provide stereo views of the chamber volume. For a real-time visual control of the streamer chamber performance during data

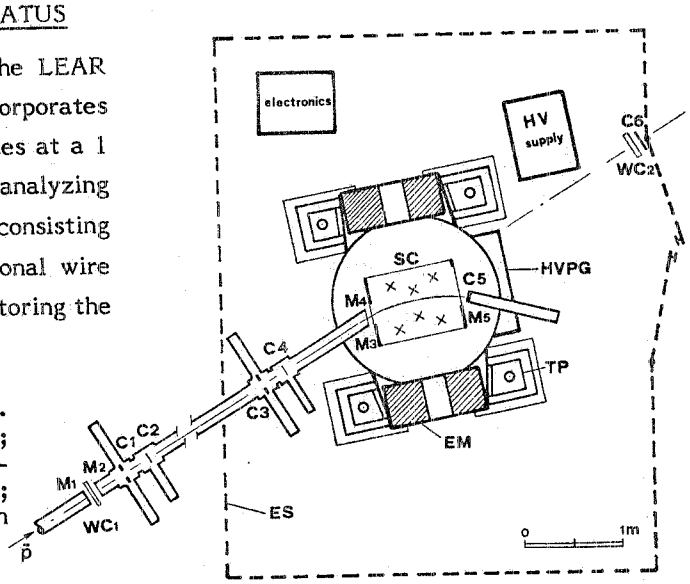

FIG. 1 - Layout of the experimental apparatus. EM-electromagnet; SC-streamer chamber; HVPG-high voltage pulse generator; TP-travelling platform; ES-electrostatic screening; WC_{1+2}-wire chambers; C_{1+6}-scintillation counters; M_{1+5}-thin walls.

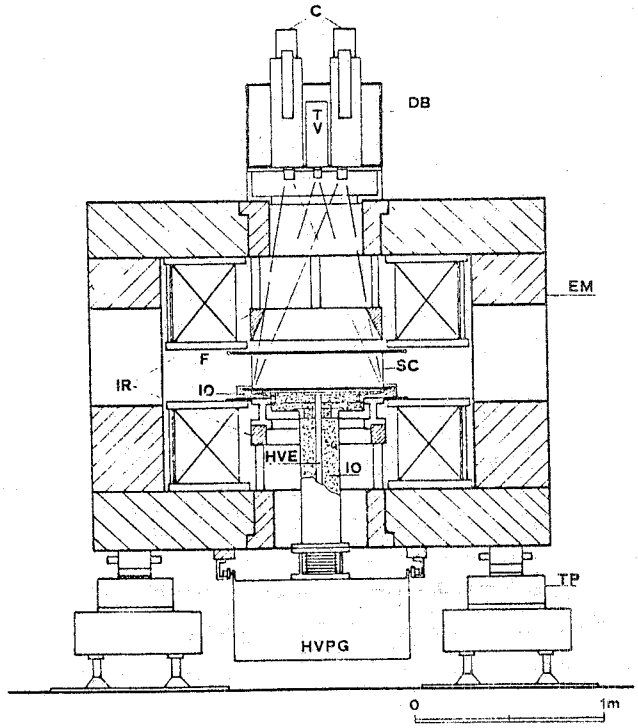

FIG. 2 - Sketch of the magnet together with the streamer chamber. SC-streamer chamber; HVPG-high voltage pulse generator; HVE-high voltage electrode; IO-insulating oil; F-light source for fiducial marks; EM-electromagnet; IR-iron rings; DB-data box; TV-television system; C-stereo cameras; TP-travelling platform.

accumulation (the beam runs) we employed a television system (TV) with image recorder which made it possible to obtain immediately some preliminary informations.

The main, essential parts of our experimental apparatus are discussed below in greater detail in the respective sections.

2.1. - The Self-Shunted Streamer Chamber

During the first part of the experiment we have utilized a streamer chamber with an inner volume of (90x70x18) cm^3. The two beam windows for the entrance (15x31) cm^2 and exit (15x41) cm^2 of the beam particles were made of 70 μm thick polyethylene (with a density of 0.94 g/cm^3). The 20 mm thick lower glass plate separating the chamber volume from the (90x70) cm^2 high voltage electrode was immersed, together with the electrode, in an insulating oil (ITE 360, AGIP) to avoid electric discharges to the surrounding metal parts of the analyzing magnet (see Fig. 2). The lateral glass walls of the chamber were 1 mm thick. The upper glass plate of the chamber, on which the ground electrode (0.1 mm wires tightened on a rectangular aluminium frame of (90x70) cm^2 with a spacing of 10 mm) is laid, has an area of (116x91) cm^2, significantly larger than the electrode itself, to prevent external surface discharges in air between the upper electrode and the high voltage electrode.

A negative voltage pulse of $\sim$140 kV was applied to the lower electrode of the chamber, and the magnetic field used was of 0.802 T. The chamber was continuously flushed with the chosen target gas (helium or neon) at a rate of about 220 litres per hour.

2.2. - The High Voltage Pulse Generator

For the operation of streamer chamber, electric pulses of a few hundreds of kV high and with special time characteristics[6] are needed. For our experiment we designed a 16 stages HVPG assembled of capacitors (Maxwell Laboratories, Inc.) of C=0.05 μF each (see Fig. 3); the resulting output capacitance of the Marx generator is C=3130 pF. The HVPG has elkonite electrodes with adjustable distances and can operate at nitrogen pressures up to 4 atm. The first section is fired by a four-electrode system (see Fig. 3), three of which are mounted at right angles to each other, while the fourth electrode consists of a platinum-iridium wire pushing on a $BaTiO_2$ pellet to provide an ultraviolet flash. This flash, seen also by the first spark gap of the generator, keeps the decay between the input and output pulses ($\sim$300 ns) fairly constant, with a negligible jitter. The trigger of the HVPG is shown in Fig. 4; it transforms the pulse from the electronic logic into the pulse required to start the generator, namely, into half the charging voltage of the generator[7]. The maximum repetion rate of the HVPG is about 8 Hz [5]. In Fig. 2 a sketch is given of the high voltage equipment placed, together with the streamer chamber, inside the electromagnet. The generator is mounted inside a (93x115x38) cm^3 iron case on four insulating plexiglas supports. The whole assembly is closed tightly with an iron lid having an opening for the connection of the generator output to the streamer chamber electrode, and then lifted into rails under the magnet. The wheels on which the HVPG is rolled into working position under the streamer chamber are fixed to the long top edges of the iron case and serve to adjust the position of the generator so that its outputs happens to be precisely opposite the centre of the high voltage electrode of the streamer chamber. The electrode (which represents a (90x70) cm^2 aluminium plate with holes 20 mm in diameter in it, made for providing a free flux of the insulating oil) is then connected to the generator; both the plate and the connection are immersed in the highly insulating oil. Thus, the iron case with the generator, together with the tube, through which the high

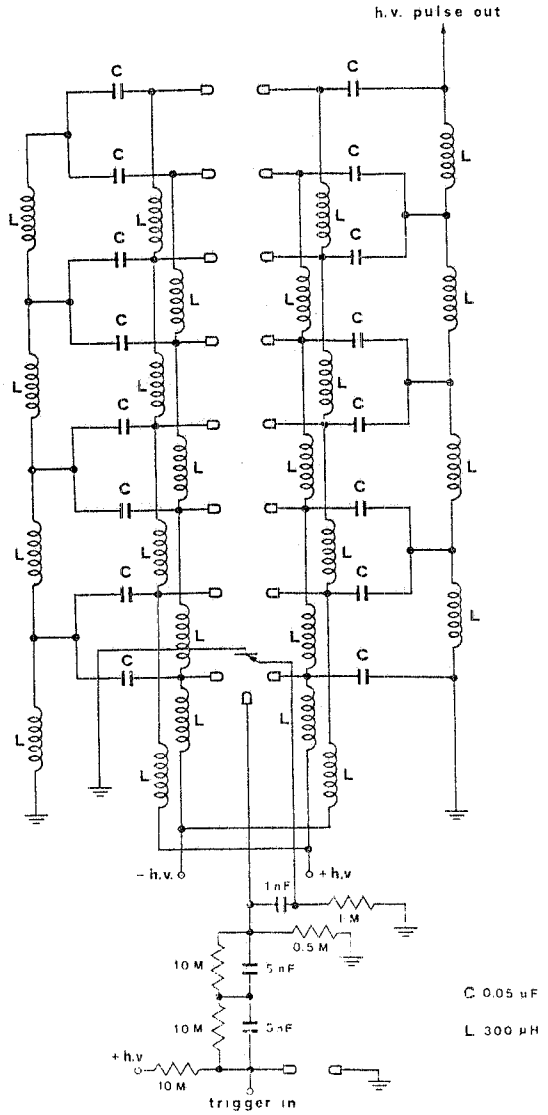

FIG. 3 - Outline of the high voltage pulse generator.

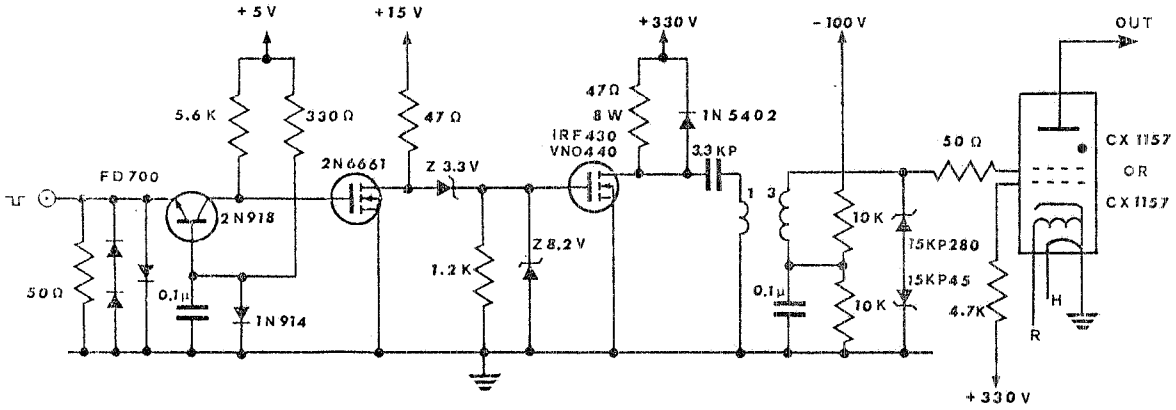

FIG. 4 - Outline of the triggering system of the high voltage pulse generator.

voltage electrode is connected to the generator, and the cup in which the electrode resides, form a combined volume filled with the insulating oil. The ground of the chamber-HVPG system is separated from the magnet's ground, which acts as first electrostatic shield.

2.3. - The Optical System

Photographs of the streamer chamber volume were taken using two cameras equipped with Leitz lenses (Summicron type; 35.06 mm/2). The optical axes of the lenses are parallel to the electric and magnetic fields, and the distance between them (the base) is 280 mm. The lenses are located 105.3 cm from the upper fiducial marks in the chamber giving a demagnification factor of 30. The mechanical film transportation system (and the charging time of the high voltage supply) permits several stereo pictures per second to be taken[8]. Fiducial marks have been engraved on the inner surface of the upper and lower glass plates of the chamber and they were illuminated by grazing flash light just after the advance of the two cameras film and photographed at the same time as the counter of pictures and the Brenner marks (the data box). The film used in our experiment was the 35 mm ILFORD HP 5, with a sensitivity of 400 ASA. The lense aperture used for photographing events occurring in helium was 2.8, permitting a good depth of field, while in the case of neon there was sufficient light for an aperture of 11.

In between the two photo cameras we installed a telecamera with a plumbicon tube (see below) for transmission and for recording of the chamber volume images to the control room of our experiment, to provide for a continuous remote visual control of the streamer chamber performance during data acquisition on magnetic tape.

2.4. - The Electromagnet

The electromagnet[9] has been built in the Frascati National Laboratories of the INFN. At present it generates a uniform (within $\pm$2%) magnetic field inside a cylindrical volume 20 cm high and 60 cm in diameter. The uniformity has been achieved by introducing two iron rings into the coils, as shown in Fig. 5.

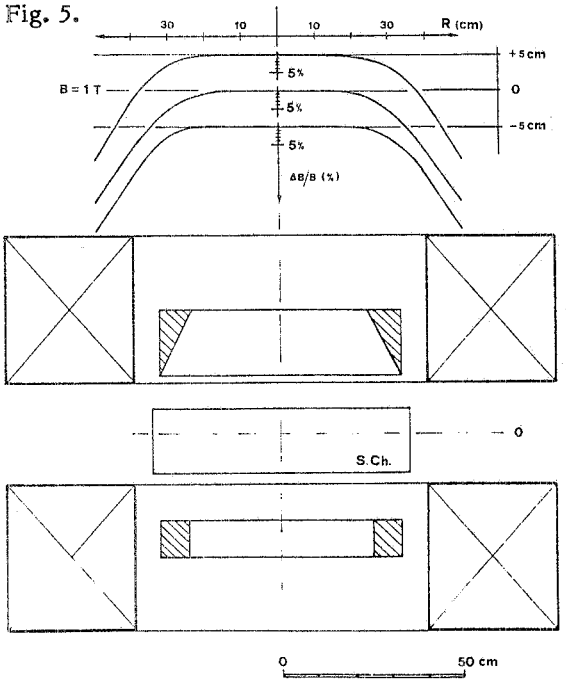

The magnet resides on four supports and by means of four air cushions can be lifted over these supports, shifted in any direction by $\pm$12 cm and rotated through about of $\pm$10°. This is essential for rapid alignment of the streamer chamber with the antiproton beam.

FIG. 5 - Layout of the electromagnet. Two iron rings introduced into the coils provide the magnetic field uniformity.

2.5. - Performance of the Chamber

In previous papers[5] we stressed that good track localization together with a high luminosity of the streamer channels forming particle tracks in a self-shunted streamer chamber are achieved by regulating the luminosity distribution along the streamer channels themselves. This is done by introducing appropriate admixtures to the main filling gas of the chamber. These quenching admixtures, amounting up to less than 0,7% do not prevent the discharge from covering the whole discharge gap, i.e. the chamber volume, but contribute to the reduction of the mean electron energy outside the neck of the discharge channel, thus reducing the light output from these parts of the discharge channels.

We have found that satisfactory tracks in a helium-filled chamber operating in a magnetic field are obtained with the use of an admixture of complex hydrocarbons at a level of $\lesssim 0.1\%$, while a neon-filled chamber requires a $\sim 1\%$ admixture of N_2.

In Fig. 6 photograph is presented of $\bar{p}$ annihilation event in helium. The lense apertures of the photo cameras were 2.8, which provided a field depth larger than the depth of the streamer chamber itself (18.1 cm). In Fig. 6 the photograph of a $\bar{p}$ annihilation event involving the production and subsequent decay a K_s^o - meson into two pions is presented. The primary and secondary vertices are clearly distinguishable from each other. In Fig. 7 a photograph of a multiparticle $\bar{p}$ annihilation event

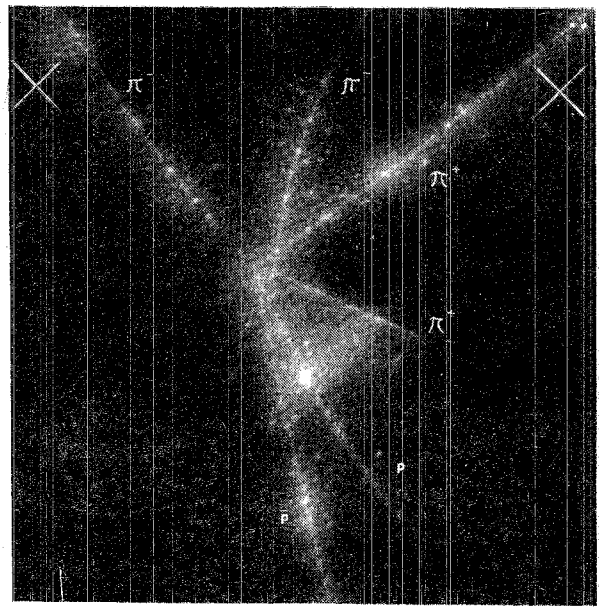

FIG. 6 - Photograph of 610 MeV/c $\bar{p}$-annihilation in flight in helium involving the production and subsequent decay of a K_s^o-meson into two pions. The distance between the central crosses is 28 cm.

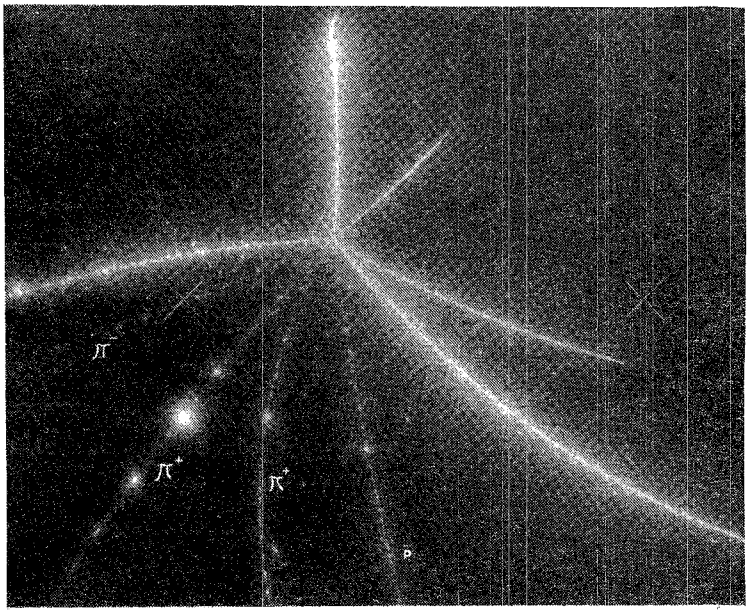

FIG. 7 - Photograph of 610 MeV/c $\bar{p}$-annihilation in flight in neon with pions and nuclear fragments emission. The distance between the central crosses is 28 cm.

in neon is shown. The tracks of 9 particles (including the incoming $\bar{p}$) with different ionization powers can be distinguished, confirming the possibility of detecting several tracks in a self-shunted streamer chamber.

The luminosity of the tracks was sufficient for the reliable operation of a television system used for continuous visual control of the chamber performance (see below). Although the luminosity of particle tracks is not proportional to the particle's ionizing power the difference in the luminosity of different tracks can certainly be utilized for an estimation of the relative ionizing powers and, consequently, for identification of the respective particles.

Thus, in our self-shunted streamer chamber it is possible to record and to identify elastic, inelastic and annihilation events and in particular to measure also very slow strongly ionizing heavy particle tracks. Neutral short time living particles, such as K°_{S} and Λ can be identified by their decay products.

3. - TRIGGERING SYSTEM

The triggering system, sketched in Fig. 1, consists of five scintillation counters: two live collimators (C_1 and C_3), two thin scintillation counters (C_2 and C_4) before the streamer chamber and one (C_5) after it. The trigger signal ($\bar{C}_1\ C_2\ \bar{C}_3\ C_4\ \bar{C}_5$) is given by each particle that, passing through the holes in the live collimators and through the thin scintillators, does not hit the final detector. This may occur as a consequence of interactions both in the filling gas of the streamer chamber (target) and in the media arranged along the beam path (scintillators, walls of the beam pipe, thin windows of the chamber, etc.).

To reduce the interactions of the antiprotons outside the chamber volume it is essential that the amount of material along the path of the beam should be at least as small as possible in comparison with the transparency of the streamer chamber (15 mg/cm^2 of He and 70 mg/cm^2 of Ne). Of course, only the trigger signals following events in the fiducial volume of the streamer chamber give us useful pictures; other triggers must be as limited as possible.

3.1. - Description of the Counters

The dimensions and arrangement of the scintillators and of the various materials on the beam line are shown in Fig. 8. The dimensions of the detectors and of the collimators optimize the efficiency of the system compatibly with the features of the LEAR beam and with the experimental area assigned to our experiment.

The entire beam telescope before the chamber is enclosed in an aluminium tube 16 cm in diameter and 400 cm long at a pressure of $\sim 10^{-3}$ torr. The tube entrance and exit are closed with thin mylar sheets and covered with an aluminium foil in order to protect the photomultipliers from room light. C_2 and C_4 are thin plastic NE104-type scintillator discs. They are placed in spherical mirrors coated with evaporated aluminium so that the light collection is higly efficient. The light from the scintillators is transmitted to the photomultipliers by conical light guides. In the C_2 and C_4 scintillators 600 MeV/c antiprotons lose 51 keV and 25.5 keV, respectively. Holes are present in the spherical reflectors to transmit the beam. They are covered with a thin aluminium foil both to increase light collection and to prevent photomultipliers from being affected by the light coming from other scintillators. A detailed description of this type of detector was given in a previous paper[10].

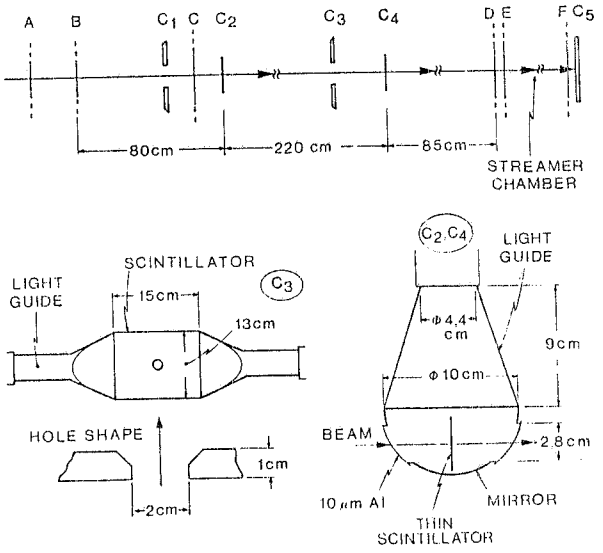

FIG. 8 - Arrangement and description of the scintillators and of the various materials on the beam line. A) End window of the LEAR beam pipe (diameter - 5 cm, thickness - 100 μm Al); B) Beam input window of our vacuum channel (4x8 cm^2, 25 μm mylar plus 10 μm Al); C) Light screening (10 μm Al); D) Output window of the vacuum channel (7.5 x 12 cm^2, 75 μm mylar plus 10 μm Al); E,F) PVC windows of the streamer chamber (thickness - 2x75 μm); C_1 and C_3 - live collimators (hole diameter: d_1=2.5 cm, d_3=2 cm); C_2 and C_4 - thin scintillators (thickness: t_2=100 μm, t_4=50 μm); C_5 - plastic scintillator (diameter - 8 cm, thickness - 0.2 cm, Al cover of 10 μ). Between D and E and between F and C_5 there are 5 cm of air. Details of the live collimators and of the thin scintillation detectors are shown.

The scintillators C_1 and C_3 are (15x10x1) cm^3 blocks in which holes 2.5 and 2 cm in diameter, respectively, have been made. The edges have a special shape which both improves the collection of the light (produced by the particles which touch the edges) and reduces the thickness of the edges (see Fig. 8). To assure high efficiency, two light guides lead from opposite sides of each scintillators to two independently operating photomultipliers. Taking into account all the matter along the beam path, it turns out that the main contribution to the beam dispersion is given by the exit window of the LEAR vacuum tube. However, with our geometry the beam spot is defined by the collimators C_1 and C_3. This assures an angular spread of not more than $\pm 0.65°$ and beam dispersion on the entrance window of the chamber of ± 2.1 cm. The aluminium foil C in Fig. 8 separates C_1 from C_3 optically.

To prevent spurious triggers, the counter C_5 must have enough acceptance to contain the "unscattered" beam, a uniformity $\simeq$ 100% and an efficiency ε such that $(1-\varepsilon) \lesssim 10^{-4}$, since the probability of interaction in the gas target is $\sim 10^{-3}$. This efficiency has to be reached before the antiprotons annihilate in the scintillator, because 4% of the annihilations produce neutral particles. Moreover, the scintillator must be relatively thin to reduce the pionic background. For these reasons a scintillator disc 1 mm thick, 8 cm in diameter has been used. It is attached to a cylindrical light guide 80 cm long in order to place the photomultiplier out from the electromagnet. The face of the scintillator in front of the beam is covered with 10 μm Al foil. High efficiency of this arrangement is obtained with a great volume of lucite, which makes the detector sensitive to the Cerenkov noise of pions. However, this effect was negligible during the first runs performed at LEAR.

3.2. - Electronics

The block diagram of the electronics is shown in Fig. 9. All the photomultipliers are PHILIPS XP2020 with CERN dividers type 4238. The constant fraction discrimination and the delayed coincidence techniques are applied to the signals coming from the detectors C_2 and C_4 to select the incoming $\bar{p}$ on the basis of their time of flight. The four coincidence signals from C_1 and C_3 are discriminated by the leading edge technique and combined in NOR logic. The signal that singles out an antiproton entering the streamer chamber is $\bar{P}_1\ \bar{P}'_1\ P_2\ \bar{P}_3\ \bar{P}'_3\ P_4 = A$. The signal produced by an antiproton hitting the counter C_5 is AP_5 and the trigger signal is $A\bar{P}_5$ (see Fig. 9).

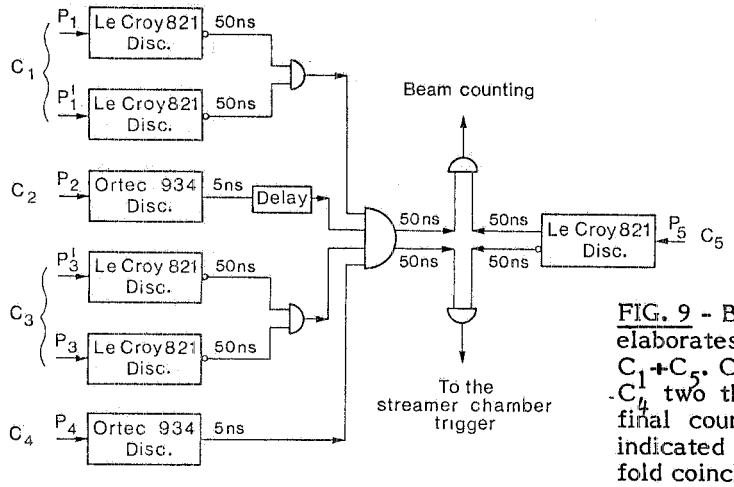

FIG. 9 - Block diagram of the electronics which elaborates the signals coming from the counters $C_1 \div C_5$. C_1 and C_3 are live collimators, C_2 and C_4 two thin scintillator detectors and C_5 the final counter. The duration of the signals is indicated in figure. The overlap time of the 4-fold coincidence is $\gtrsim$ 2 ns.

Fig. 10 shown the charge spectra of the thin scintillator detectors. The 600 MeV/c $\bar{p}$ signals, formed by 10-20 photoelectrons, are clearly distinct from the background current of the photomultipliers. In the presence of the beam the number of background signals increased with the

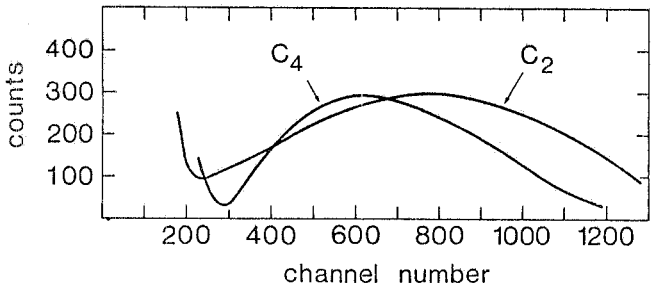

FIG. 10 - Charge spectra for the thin scintillator detectors. Energy loss in C_3 is 51 keV and in C_4 is 25.5 keV. Conversation factor is 0.125 pC/channel.

beam intensity, probably due to the delayed component of the scintillator light pulses[11] and to multiple light reflections in the scintillator and in the reflector or in the light guide. To avoid casual coincidences, the discriminator threshold of C_2 and C_4 has been fixed very far from the background, reducing slightly the intensity of the detected beam.

The prompt time spectrum of the discriminated signals from C_2 and C_4 was obtained with a SILENA 7412 time to amplitude converter having a 50 ps/channel resolution. This spectrum has a gaussian shape with small deviations on the tails and shows a FWHM of 1.5 ns. On the basis of previous studies of thin scintillators detectors[12], this time jitter may be due mainly to fluctuations in the energy lost in the scintillators, with minor contributions arising from the scintillator light emission spectrum, the photomultipliers and the size of the detectors. The curve obtained by counting the coincidences between C_2 and C_4 as a function of the delay of C_2 showed a FWHM of 5 ns and a plateau of causal coincidences of relative weight $\leq 5 \times 10^{-4}$.

3.3. - Efficiency

The antiprotons undergo single and multiple Coulomb scattering, elastic and inelastic nuclear scattering and annihilation. All the interactions contribute to the production of spurious photographs, while only the nuclear scattering and the annihilation inside the streamer chamber give useful pictures.

The Coulomb interactions produce an angular spread of the incident beam at small angles. Part of the particles scattered before the detector C_3 are removed by the live collimators C_1 and C_3. The rest, together with the particles deviated after C_3, must hit the final detector C_5.

Antiproton interaction events affect the trigger depending on the region where they occur.

i) Region before C_4. The interactions remove antiprotons from the beam, but spurious triggers may be given by secondary pions produced in the annihilations[13]; however, due to the delayed coincidence between C_2 and C_4 and to the presence of the live collimators these cases are rare.

ii) Region between C_4 and the gas target. The interactions in this case produce blank pictures or pictures also with tracks off the beam line.

iii) Region after the gas target. If the charged particles emitted in the interactions do not hit scintillator C_5 or if they do not release sufficient energy in C_5, photographs of antiproton undeviated tracks are produced.

iv) Region inside the streamer chamber (gas target). These interactions produce useful events, but if a particle from the reaction is detected by C_5, the picture is not taken. Taking into account the solid angle covered by C_5, this occurrence has a probability at most of about 4×10^{-3}.

The efficiency of the trigger system may be evaluated by the ratio between the number of pictures containing useful events (N_{ev}) and the total number of pictures (N_p). Also it is useful to know the ratio between N_p and the number of antiprotons (N_5) hitting the final scintillator. For the sake of convenience instead of N_{ev} the number N_{ev}^{in} of the inelastic events will be considered.

The effects dependent on the Coulomb multiple scattering and on the beam geometry were studied by adapting the Monte Carlo program GEANT[14] to our experiment. To evaluate the effects dependent on nuclear interaction, we used cross sections from the literature or extrapolated from them[15]. For the arrangement of Fig. 8 our evaluations for a fiducial gas 55 cm long target give:

$N_{ev}^{in}/N_p \simeq 0.12$ $\qquad$ $N_p/N_5 \simeq 2.6 \times 10^{-3}$ for ^4He

$N_{ev}^{in}/N_p \simeq 0.20$ $\qquad$ $N_p/N_5 \simeq 3.7 \times 10^{-3}$ for ^{20}Ne

During the runs at LEAR we obtained:

$N_{ev}^{in}/N_p \simeq 0.08$ $\qquad$ $N_p/N_5 \simeq 3\text{-}4 \times 10^{-3}$ for ^4He

$N_{ev}^{in}/N_p \simeq 0.14$ $\qquad$ $N_p/N_5 \simeq 5\text{-}6 \times 10^{-3}$ for ^{20}Ne

The agreement between the evaluations and the experimental values is fairly good, considering the uncertainties in the values of the cross sections we used and in the evaluation of the Coulomb scattering effects.

The fluctuations observed for the N_p/N_5 values may be attributed to a not constant position of the incoming beam and to the lack of efficiency of the live collimator C_3 in detecting antiprotons lightly touching the edges of the hole. When the beam is perfectly aligned, the ratio N_p/N_5 is minimal, but when it is not well aligned more antiprotons graze the edges of the holes in the counters and are deviated without releasing enough energy to be detected. In these conditions more particles are scattered to an angle small enough to be detected by C_4 but too large to be detected by C_5. Thus, the ratio N_p/N_5 becomes higher.

The effect due to the insensitivity of the edges of the live collimators is difficult to study quantitatively. However, it has been proved experimentally by changing the high voltage of the two

photomultipliers, which look independently at the edges of the hole of C_3, from 2700 V (plateau value) down to 2200 V. An increase in the ratio N_p/N_5 by a factor of 2÷3 was observed.

The efficiency of detector C_5 was tested by using for this counter two different scintillators, one 1 mm thick and one 2 mm thick. No change was observed and it is possible to conclude that the efficiency defect of this detector is less than 10^{-4}.

We also note that no appreciable background of secondary pions has been observed in the coincidence curve between the thin scintillators C_2 and C_4 and in the spectrum of detector C_5, showing that the efficiency experimental values are not contaminated by this effect.

4. - VISUAL CONTROL OF THE STREAMER CHAMBER PERFORMANCE USING A TV CAMERA SYSTEM

It is shown in Ref. (16), that a continuous visual control of the self-shunted streamer chamber performance using a television system is possible owing to the high luminosity of particle tracks in the chamber. In our experiment we utilized the telecamera with a plumbicon tube, characterized by a low dark current, high sensitivity, and the possibility of rapid cancellation of a previous record. We obtained a 100% track registration efficiency with respect to parallel track detection using photo cameras. The good quality of the detection system is illustrated by the photograph of an event from the television set screen presented in Fig. 11.

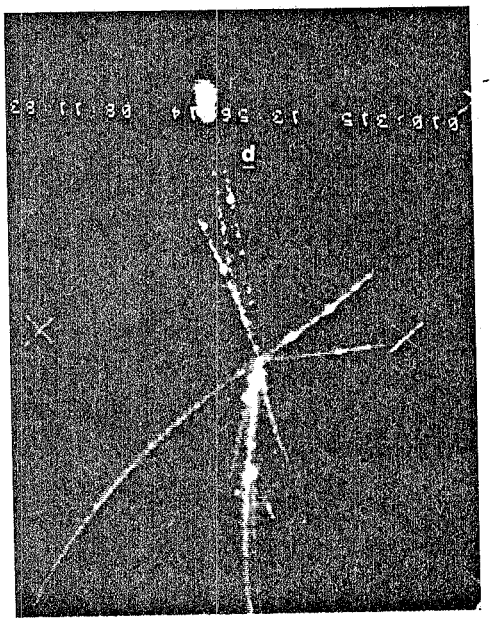

FIG. 11 - Antiproton annihilation event in neon photographed on the monitor of the TV control system.

An important characteristic of this TV system control is the possibility of storing the single TV field (corresponding to one photograph in the film) in a TV recorder when the magnetic tape is stationary. The advancement of the tape of one field is possible every time the master trigger from the electronics of the environmental apparatus arrives. Thus the TV images are stored, one field per one event, sequentially without loss of tape. The synchronization of the TV recorder with telecamera is obtained exploiting the storing properties of the plumbicon tube; in fact the event image can be read in the plumbicon target only when the recorder is ready for writing. Obviously the scanning beam of the plumbicon tube is blancked during the time between the arrival of the master trigger and the arrival of the next field after the ready signal from the videorecorder. Until the arrival of the next master trigger the magnetic tape is stopped and the last stored image is continuosly read, in playback, and displayed in a TV monitor. In this manner it is possible to have a more useful control of the streamer chamber operation.

All the TV images are electronically labelled through a time data generator and a trigger counter (see bottom of Fig. 11); then the research of the single images in playback is very facilitated.

The maximum frequency of the single field recording is one field per second, using our videorecorder (1" Grundig BK 411 HE with the remote control FB 400 E). The playback of the field sequence may be released manually or by means of an external keying unit providing a maximum repetition frequency of 1 field per second. For this single field storage option a camera without interface is required.

When a single field is displayed from the videorecorder, the same field is continuously scanned, thus one frame in the TV monitor is arranged by two equal fields.

The used telecamera is the Grundig FA70H (bandwith 20 MHz) with 1" plumbicon tube XQ1353.

Some little modifications to the telecamera and to the videorecorder were necessary to perform the synchronization master trigger-telecamera-videorecorder.

A magnetic shielding (an iron-metal box) of the telecamera was necessary to prevent interference by the dispersed magnetic field from the electromagnet. This shielding box was cooled by a flow of compressed air at ambient temperature. The videorecorder with the control, the TV monitor and the electronic data box were out of the Faraday cage containing the experimental apparatus at a distance of about 40 m. All the connections between the TV system out of the Faraday cage and the telecamera were done by optic fiber links to prevent electromagnetic troubles from the high voltage pulse generator. The bandwith of the videorecorder was 10 MHz.

5. - CONCLUSIONS

The results of the first run of a self-shunted streamer chamber in a magnetic field at LEAR clearly demonstrate the broad facilities that this experimental technique provides for nuclear physics studies with low-energy antiproton beams involving the production of many relativistic and nonrelativistic particles and nuclear recoils.

Our future intentions are to continue the systematic investigation of the interaction between low-energy antiprotons and the ^{2}H, ^{3}He, ^{4}He, Ne nuclei.

6. - ACKNOWLEDGEMENTS

We wish to express our gratitude to the LEAR and South Hall area teams for their continuous support. We are grateful to V.P. Dzhelepov, S.A. Nunyatov, M.B. Pontecorvo, R. Garfagnini and R. Scrimaglio for their contant interest and support in this work and to C. Milani for her participation to the first part of the experiment.

We are grateful to the large number of people who have been involved in the construction of this experiment. We wish to thank in particular:

at Frascati National Laboratory: B. Dulach, S. Fontana and the Mechanical Project Office; F. Sgamma, A. Vitali and the Mechanical Workshop; S. Faini and the Mechanics and Vacuum Service; M. Albicocco, W. Pesci, A. Orlandi and A. Viticchiè of the LEALE staff for the technical and engineering work in rebuilding the magnet and of the centering system on the beam;

at the Physics Department of the Pavia University: P.L. Beltrami, S. Bricola, L. Cecco, G. Juvino and A. Vicini for the design and construction of photocameras and triggering system;

at the Physics Institute of Torino University: A. Beninati, A. Callà, M. Menegazzo, A. Pia, L. Simonetti, L. Valsasna and the Electronic Workshop for the design and construction of the system and of the Faraday cage.

REFERENCES

(1) Proc. Workshop on Physics at LEAR with Low-Energy Cooled Antiprotons, Erice, 1982 (Eds. U. Gastaldi and R. Klapisch) Plenum press, (1983).
(2) Dubna-Frascati-Padova-Pavia-Torino collaboration, F. Balestra et al., CERN/PSCC/80-78, PSCC/P17 with Add. 1; CERN/PSCC/83-34, PSCC/17/M164.
(3) V.M. Chechetkin, M. Yu. Khlopov and M.G. Sapozhnikov, Riv. Nuovo Cimento 5, 1 (1983).
(4) I.V. Falomkin, G.B. Pontecorvo, M.G. Sapozhnikov, F. Balestra and G. Piragino, Nuovo Cimento 79A, 193 (1984).
(5) F. Balestra, L. Busso, R. Garfagnini, G. Perno, G. Piragino, R. Barbini, C. Guaraldo, R. Scrimaglio, I.V. Falomkin, M.M. Kulyukin, G.B. Pontecorvo and Yu. A. Shcherbakov, Nuclear Instr. & Meth. 125, 157 (1975).
(6) I.V. Falomkin, M.M. Kulyukin, G.B. Pontecorvo, V.M. Soroko and Yu. A. Shcherbakov, preprint JINR, P13-6533 (1972).
(7) A. Beninati, L. Busso, D. Panzieri and F. Tosello, Nuclear Instr. & Meth., in press.
(8) C. Marciano, preprint CERN, in preparation.
(9) P.E. Argan, A. Gigli, E. Picasso, V. Bisi, G. Piragino, G. Bendiscioli and A. Piazzoli, Nuovo Cimento Suppl. 17, 215 (1960).
(10) G. Bendiscioli, V. Filippini, G. Fumagalli, E. Lodi Rizzini, C. Marciano, C. Milani, A. Rotondi and A. Venaglioni, Nuclear Instr. & Meth 206, 471 (1983).
(11) F.D. Brooks, Nuclear Instr. & Meth. 162, 477 (1979).
(12) T. Batsch and M. Moszynsky, Nucl. Instr. & Meth 123, 341 (1975).
(13) A.G. Ekspong, A. Frisk, S. Nilsson and B.E. Ronne, Nucl. Phys. 22, 353 (1961).
(14) R. Brun, F. Carena, M. Hansroul, J.C. Lassalle, G.N. Patrick, CERN/DD/US/06.
(15) G. Bendiscioli, G. Fumagalli, C. Milani, A. Rotondi, R. Tidori, A. Venaglioni and A. Zenoni, preprint TOFRADUPP/INFUP/BE-07/82, unpublished.
(16) A. Cavestro, M. Schiavon, M. Vascon, G. Zanella, F. Balestra, L. Busso and G. Piragino, Nucl. Instr. & Meth. 188, 69 (1981).